Journal Name

ARTICLE TYPE

Cite this: DOI: 00.0000/xxxxxxxxxx

Entropy in catalyst dynamics under confinement†

Qi-Yuan Fan,[a,b,‡] Yun-Pei Liu,[a,‡] Hao-Xuan Zhu,[a,‡] Fu-Qiang Gong,[a] Ye Wang,[a] Weinan E,[c,d] Xinhe Bao,[e] Zhong-Qun Tian[a,f] and Jun Cheng*[,a,f,g]

Method

Training of machine learning potential

In this work, the machine learning potentials (MLPs) are constructed based on the Deep Potential Generator (DP-GEN) package[1], which involves a series of successive iterations. Each iteration includes three steps: exploration, labeling, and training. The smooth version was adopted to train the MLPs in the present work[2]. The detailed network parameters of the training step are set as follows: the sizes of the embedding net and fitting network are set as (25, 50, 100) and (240, 240, 240), respectively. The learning rate of the neutral network starts at 10^{-3} and decays exponentially to 10^{-8}. The neutral network of each iteration is trained with 400,000 steps, while the MLP model in the last iteration is trained with 4,000,000 steps. The cutoff radius for neighbor searching is set to 7 Å, and the start radius of smooth is set to 0.5 Å. Four MLPs are trained here, with the same network architecture but a different random initial seed.

Machine learning molecular dynamics

The exploration step of the workflow is carried out using the LAMMPS code based on the generated MLP. In this work, our initial training data set consists of only a few initial and final state structures, which are randomly selected from the ∼5 ps AIMD trajectories at 800 K. To calculate the reaction free energy, it is essential to sample different points along the predefined reaction coordinate. Thus, we perform a series of restrained MD simulations along the predefined reaction coordinate (i.e., O-O bond length) at various temperatures. We gradually vary the O-O bond length in increments ranging from 0.1 to 0.3 Å at different temperatures to obtain the structures around the transition states. Specifically, in the case of O_2 dissociation on the bare Pt_{15} cluster, we explore the configurational space at seven different temperatures varying from 200 to 1400 K with an interval of 200 K. The O-O bond lengths change from 1.35 to 1.83 Å, and the distance intervals are small, 0.1 Å. While at O-O distances between 1.83 and 6.33 Å, the increments are set to 0.3 Å. Similarly, for the O_2 dissociation on the Pt_{15} cluster confined inside a carbon nanotube (Pt_{15}@CNT), the chosen CNT (7,7) substrate here has a diameter of ∼0.97 nm, a length of ∼1.97 nm, and a number of C atoms 224, has ten temperatures, varying from 100 to 1000 K at intervals of 100 K, and the restrained MD was performed along the O-O bond length ranging from 1.2 to 4.0 Å in 0.3 Å intervals. The MLP model of O_2 dissociation on Pt_{15} cluster supported outside carbon nanotube (Pt_{15}/CNT) includes 11 temperatures varying from 200 to 1200 K at 100 K intervals, and the O-O bond lengths ranging from 1.4 to 4.1 Å at intervals of 0.3 Å. For the calculations of Pt_{27}@CNT and Pt_{36}@CNT system, the CNT(8,8) with a diameter of ∼1.1 nm and a length of ∼2.5 nm and CNT(9,9) with a diameter of ∼1.2 nm and a length of ∼2.5 nm are chosen as the substrate, respectively, which ensures that the clusters are fully encapsulated in the channel. In calculating the free energy profiles of O_2 dissociation on Pt_{27}@CNT at different temperatures, more than 15 O-O bond lengths are constrained along the reaction coordinate at each temperature.

During the exploration step, to select structures for labeling, here, we use the model deviation (σ_f^{max}) reported by Zhang et al.[1,3] as an error indicator, which is defined as the maximum standard deviation of the atomic forces predicted from the four neutral network model, the equation is as follows:

$$\sigma_f^{max} = {}_i^{max} \sqrt{\left\langle \left\| f_i - \bar{f}_i \right\|^2 \right\rangle}, \bar{f}_i = \langle f_i \rangle \quad (1)$$

in which the f_i represents the force applied on atom i, $\langle f_i \rangle$ denotes the ensemble average predicted by the MLP models. During the exploration step, we define an upper and lower bound of the trust levels. When those σ_f^{max} falls in the range of 0.2 to 0.5 eV/Å the corresponding configurations are considered as candidates for labeling, followed by DFT calculations, and are incorporated into the data sets. In each iteration, MD runs are applied using previously trained MLPs. The final MLP requires more than 99% of the configurations to reach the set lower bound of the model deviation.

DFT calculations

In the labeling step of the workflow, we use the Vienna Ab initio Simulation Package (VASP)[4,5] to generate the energies and forces. The detailed calculation setup is as follows, the interaction between the ion and electron was characterized by the projector-augmented wave (PAW) method[6,7]. The exchange-correlation energies of electrons were treated with the Perdew-Burke-Ernzerhof (PBE) functional[8]. The cutoff energy of the plane-wave basis set was set as 600 eV, and the energy and force convergence criteria were set as 10^{-7} eV and 0.001 eV/Å, respectively. In calculations, the Pt_{15} and Pt_{27} clusters were placed in a cubic box of 18×18×18 $Å^3$, and the Pt_{36} clusters were placed

in a large cubic box of 24×24×24 Å^3. For the Pt_{15}@CNT, the side lengths of the cube are 20, 20, and 19.6761 Å, and for the Pt_{15}/CNT, the cubic box with a side length of 25×25×19.6761 Å. For the Pt_{27}@CNT and Pt_{36}@CNT systems, the side lengths of the cube are set to 20, 20, and 24.5951 Å.

Free energy calculations

The final free energy calculations were performed using a modified version of the CP2K package with a DeepMD-kit interface [9] based on the well-trained MLP model. The free energies are obtained from computing the potential of mean force (PMF) [10] along a pre-defined reaction coordinate. For a forming/breaking bond reaction, the most popular choice of reaction coordinate is the distance between two atoms [11–13]. Here, we choose the O-O bond length as the reaction coordinate to calculate the free energy profile of O_2 dissociation. It is an appropriate reaction coordinate because this collective variable (CV) separates all states along the reaction pathway and satisfies the guidelines for selecting CVs suggested by Parrinello [14].

In this work, the PMF is calculated by the Lagrange multiplier algorithm. Briefly, by deriving the free energy $A(\xi)$ in terms of the reaction coordinate ξ, we can get $\frac{dA}{d\xi} = \left\langle \frac{\delta H_\xi^F}{d\xi} \right\rangle$, where the H_ξ^F is the Fixman Hamiltonian with respect to the generalized coordinates, and the derivative of the Hamiltonian versus ξ can be viewed as an external force acting in the system to keep the reaction coordinate constant.

To obtain the reaction free energies and barriers, we performed a series of constrained MD simulations to calculate the mean forces for a set of O-O bond lengths at a given temperature. The temperatures are maintained using the canonical sampling through velocity rescaling (CSVR) [15] thermostat applied in a canonical ensemble (NVT) ensemble. The time step of MD was set to 0.5 fs. In the PMF curves, the three points with zero force with the increase of O-O bond length correspond to the initial (IS), transition (TS), and final states (FS), respectively. Then, we can obtain the free energy profiles by integrating the mean forces over the O-O bond length.

Estimate of statistical errors in free energy calculations

To assess the accuracy of our MLMD calculations, we employ a block averaging technique to estimate the errors associated with average forces and free energies at each O-O bond length. This statistical analysis involves the following step:

1. Dividing the equilibrated MLMD trajectories into five evenly spaced time intervals.
2. Calculating the forces and free energies for each of these time intervals independently.
3. Determining the standard deviations across these five intervals.

These standard deviations are then utilized as the corresponding statistical errors, providing a quantitative measure of the uncertainty in our calculated values.

Structural analysis

Solid-to-liquid phase transition

In this study, the structural descriptor, root-mean-squared Pt-Pt bond length fluctuations (δ_{rms}), is used to illustrate the phase transition behaviors of clusters. The δ_{rms} is calculated using the following formula (S2) [16]:

$$\delta_{rms} = \frac{2}{n(n-1)} \sum_{i<j} \frac{\left\langle r_{ij}^2 \right\rangle - \left\langle r_{ij} \right\rangle^2}{\left\langle r_{ij} \right\rangle} \tag{2}$$

where n represents the number of Pt atoms in the cluster, r_{ij} represents the Pt-Pt bond length, and $\langle ... \rangle$denotes an average over the MLMD trajectory.

There are three regions in the δ_{rms} curves: the first one at a lower temperature is the solid-like region, in which the Pt atoms vibrate around their equilibrium positions, and hence, δ_{rms} has a minor change. In comparison, the one at a higher temperature is the liquid-like region, where the clusters mainly exist as high-energy isomers that more strongly vibrate around their equilibrium positions, giving a more appreciable increase in δ_{rms}. As for the phase coexistent region, the clusters gradually transform from a solid-like to a liquid-like state. Thus, a significant bond length fluctuation is observed.

Coordination number

To characterize the configurations in MLMD trajectories, we analyze the average coordination number (CN). The CN is defined as [17]

$$CN(i) = \sum_j \frac{1 - (\frac{r_{ij}}{r_0})^n}{1 - (\frac{r_{ij}}{r_0})^m} \tag{3}$$

in which r_{ij} denotes the measured interatomic distance, and r_0 represents the cutoff distance. The cutoff value is set to be 3.2 Å for Pt-Pt and 2.6 Å for Pt-C bond length. The exponential factors n and m are set to 6 and 12, respectively.

Root-mean-square deviation

To measure the dissimilarity of the trajectory conformational ensemble, we analyze the root-mean-square deviation (RMSD) using the MDAnalysis toolkit in Python, which can be obtained using the following formula (S4) [18]

$$RMSD = \sqrt{\frac{\sum_{i=1}^{n} (x_i - x_i^r)^2}{N_A}} \tag{4}$$

where x_i are the coordinates of atom i, N_A is the number of atoms in the cluster, and x_i^r is the coordinates of the reference frame. In this work, the reference is the first frame of the MLMD trajectory.

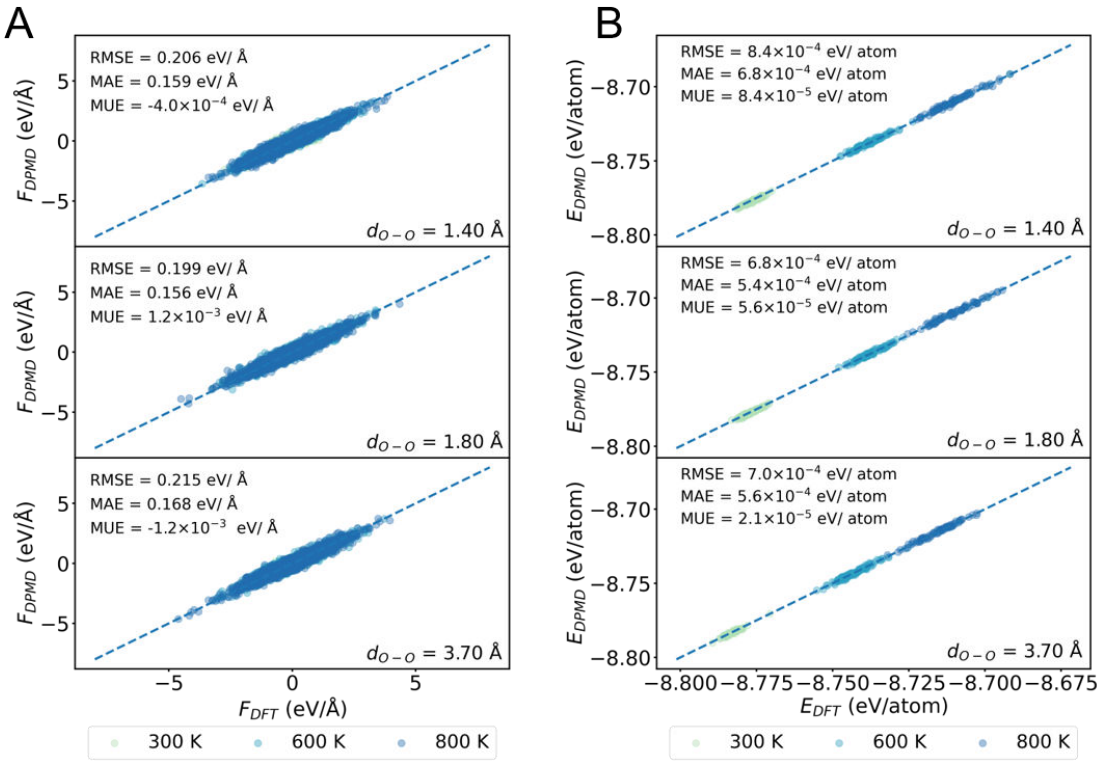

Fig. S 1 The comparison between the forces (A) and energies (B) for O_2 dissociation on the Pt_{15}@CNT along the O-O bond length at different temperatures predicted by the MLP and that calculated from DFT. The insets represent the error towards force and energy for validation data.

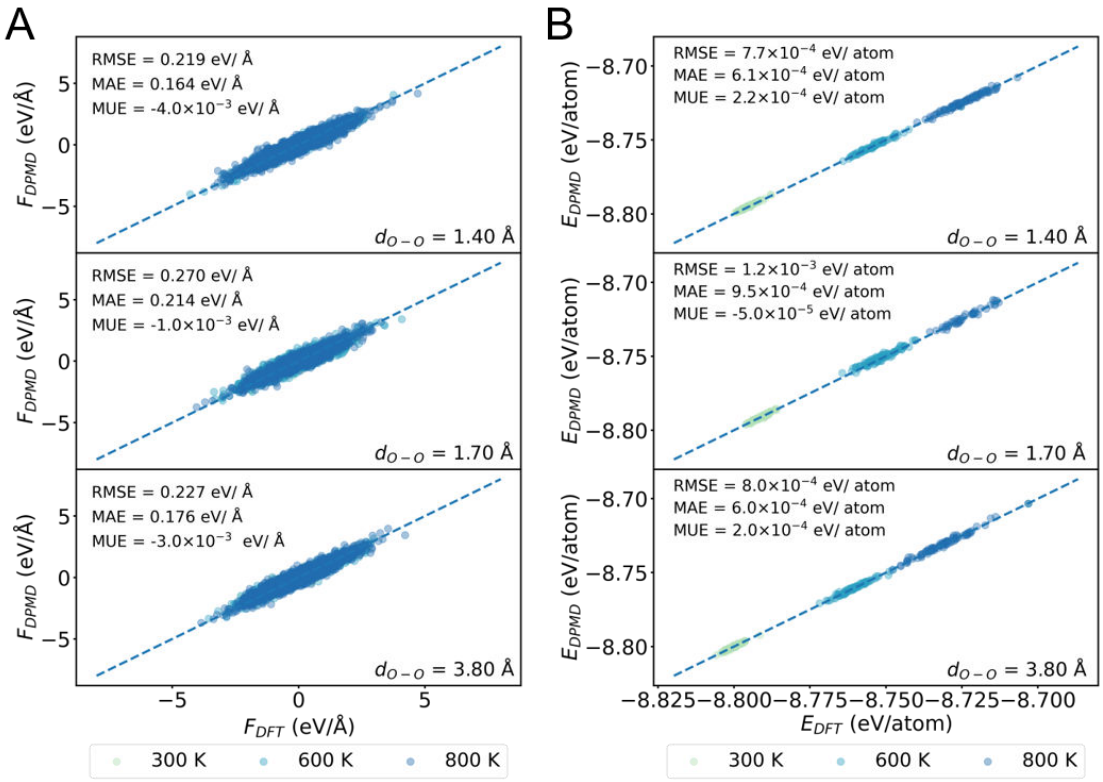

Fig. S 2 The comparison between the atomic forces (A) and energies (B) for O_2 dissociation on the Pt_{15}/CNT along the O-O bond length at different temperatures predicted by the MLP and that calculated from DFT. The insets represent the error towards force and energy for validation data.

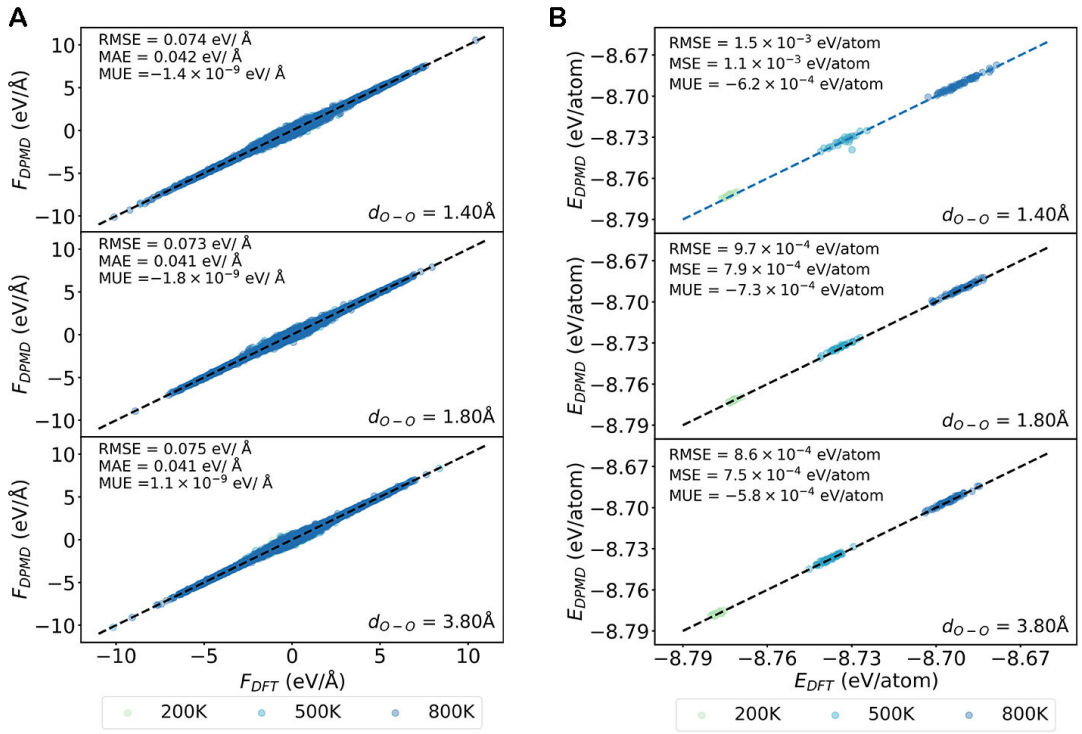

Fig. S 3 The comparison between the atomic forces (A) and energies (B) for O_2 dissociation on the Pt_{27}@CNT along the O-O bond length at different temperatures predicted by the MLP and that calculated from DFT. The insets represent the error towards force and energy for validation data.

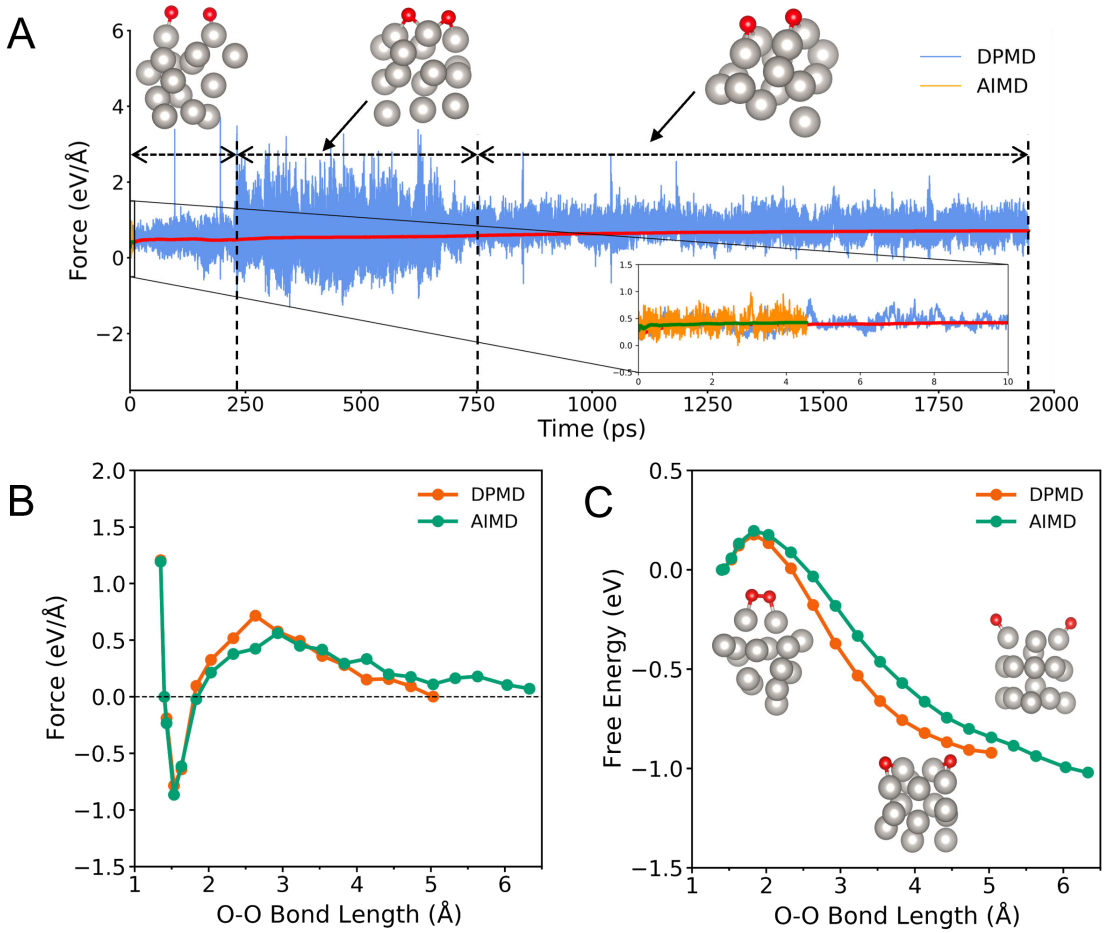

Fig. S 4 (A) Time accumulative averages of the forces at the O-O bond length of 2.63 Å at 673 K calculated using MLMD and AIMD. The insets are representative snapshots of structures with the simulated time selected from the MLMD trajectory at 673 K. The silver and red balls in structures are Pt and O atoms. (B) The PMF curves of O_2 dissociation on Pt_{15} cluster at 673 K calculated using MLMD and AIMD. (B) The corresponding free energies profiles of O_2 dissociation on Pt_{15} cluster at 673 K obtained using MLMD and AIMD.

Note: At the same time scale of ~5 ps, the mean forces derived from machine learning accelerated molecular dynamics (MLMD) and AIMD exhibit good agreement. However, when extending to the longer time scale, the mean forces obtained by MLMD converge to a different value, indicating the insufficient timescale of AIMD for describing structural dynamics. Specifically, for time scales between 250-750 ps, two O atoms adsorbed on the bridge site and coordinated to three Pt atoms, and when the time scale was greater than 750 ps, two O atoms were coordinated to four Pt atoms. Whereas, when the time scale is less than 250 ps, the O atoms adsorbed on top site. This indicates that only the configurations of the O atoms adsorbed on the top site can be captured on the AIMD scale of 5-10 ps.

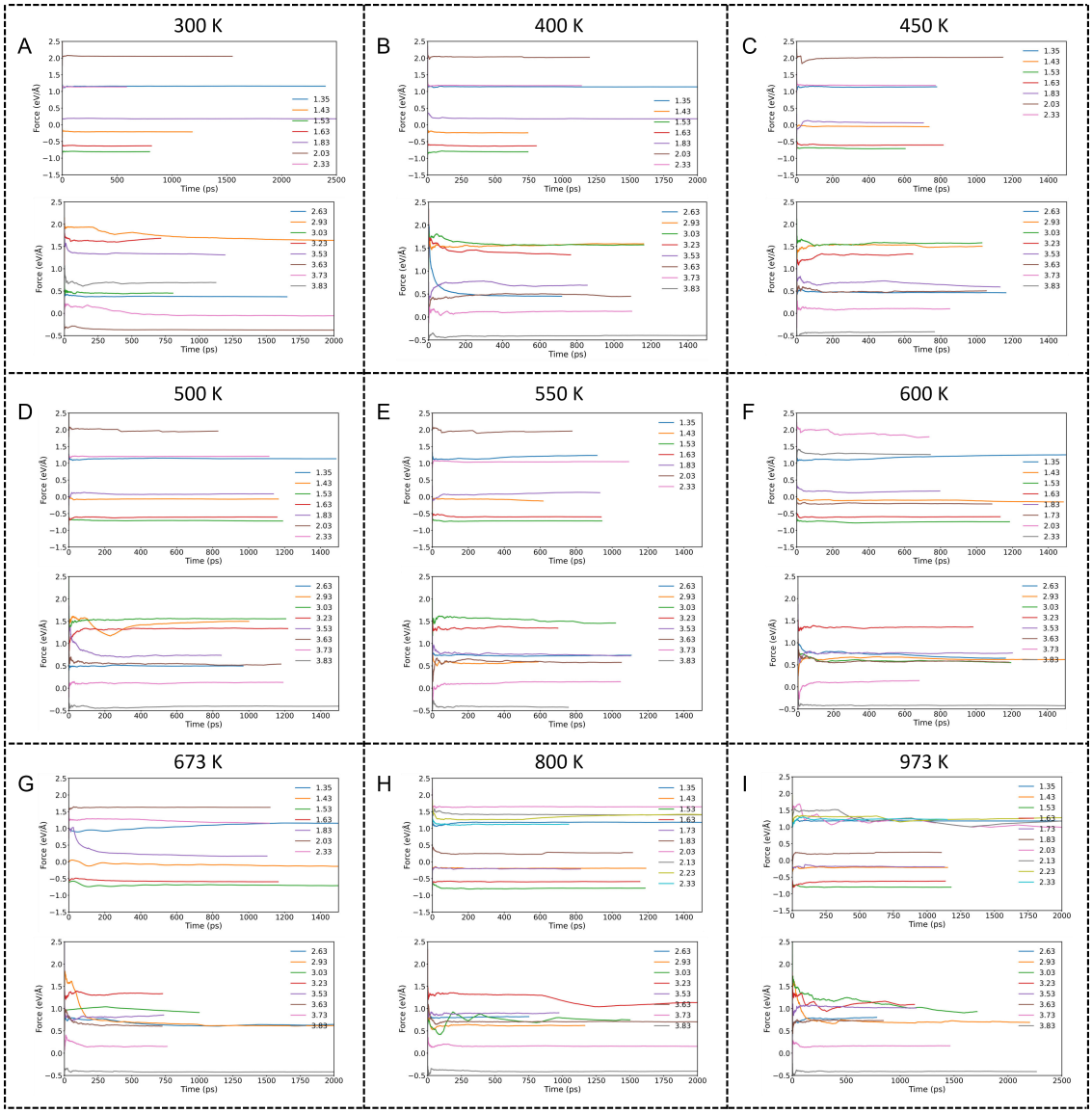

Fig. S 5 Time accumulative averages of the forces of O_2 dissociation on Pt_{15} cluster at the O-O bond length varying from 1.35 to 3.83 Å at different temperatures calculated by MLMD. The insets are O-O bond length given in Å.

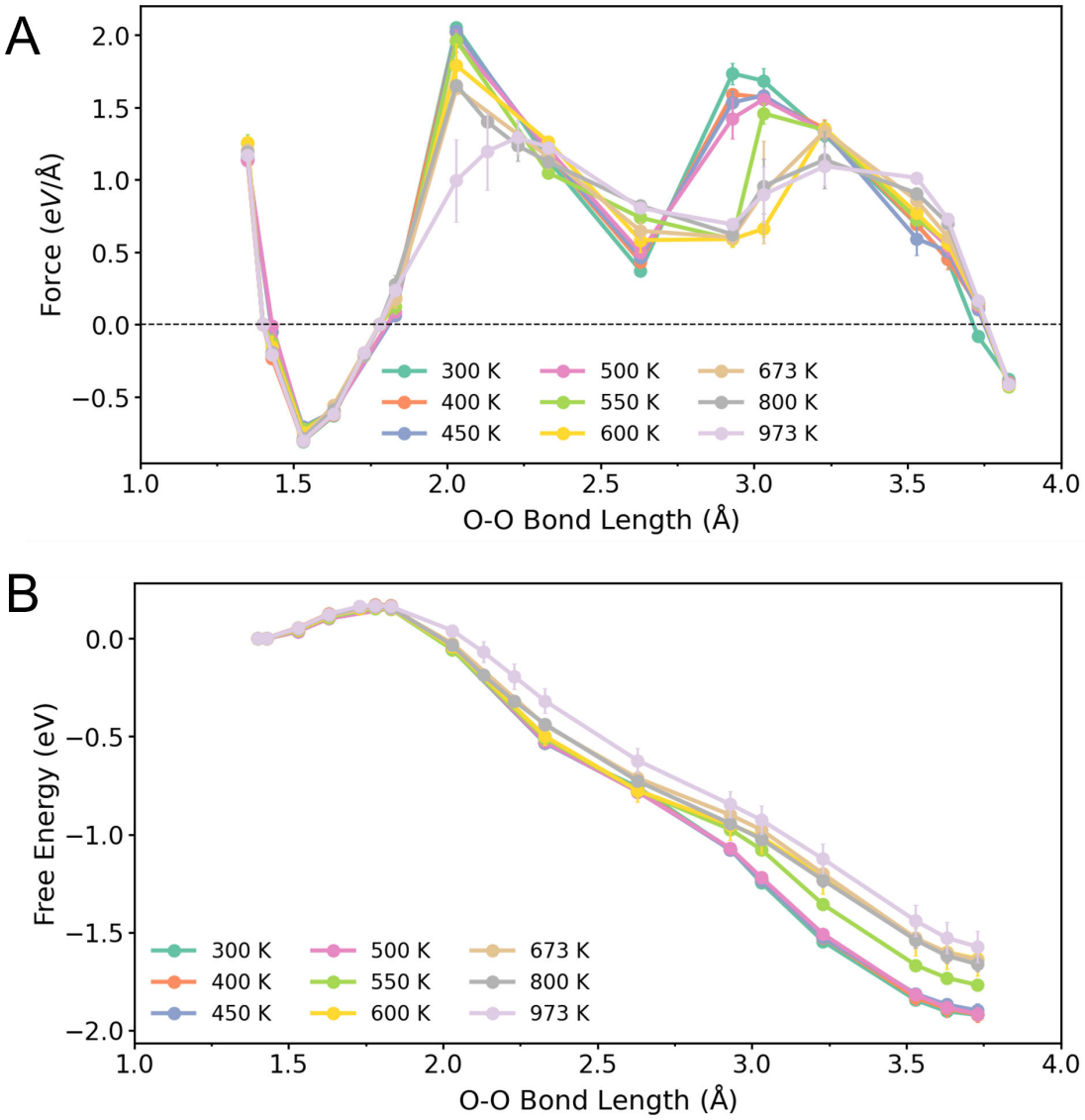

Fig. S 6 Calculated mean forces (A) and free energy profiles with error bars (B) for O_2 dissociation on Pt_{15} cluster along the O-O bond length at different temperatures calculated using MLMD. The insets are the corresponding temperatures.

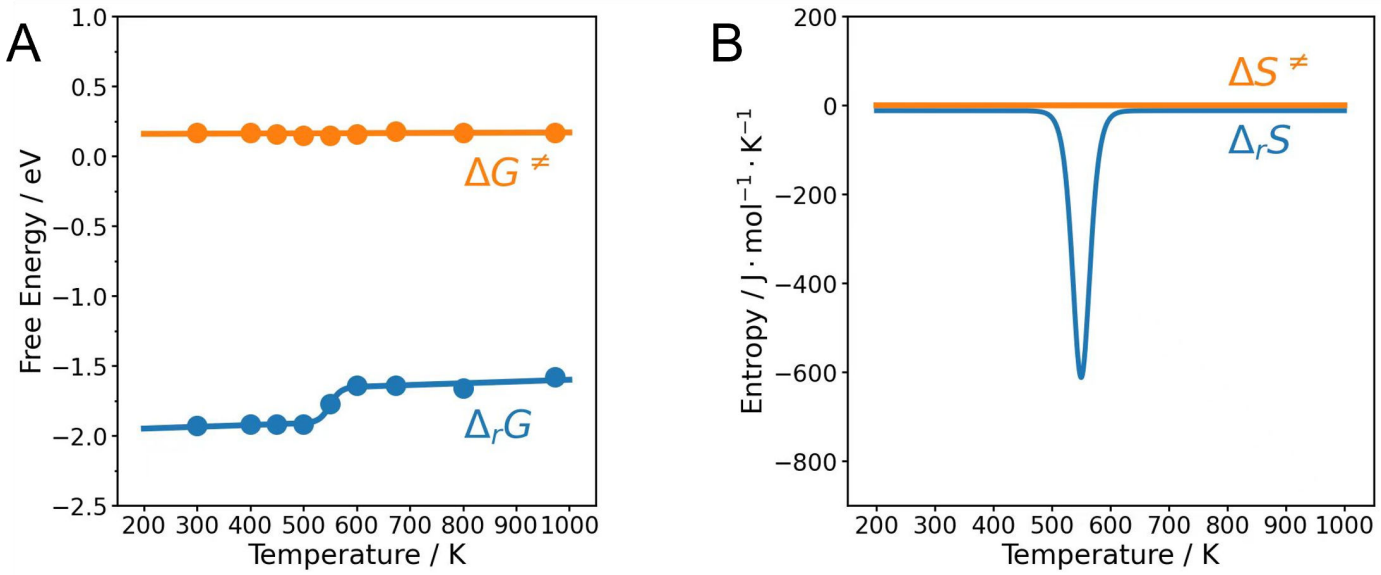

Fig. S 7 (A) The reaction free energy (Δ_rG) and barrier ($\Delta G^{\neq}$) of O_2 dissociation on Pt_{15} cluster as a function of temperature. The points represent the calculated values, and the lines are corresponding fitted curves. (B) The reaction entropy change (Δ_rS) and activation entropy ($\Delta S^{\neq}$) of O_2 dissociation on Pt_{15} cluster as a function of temperature.

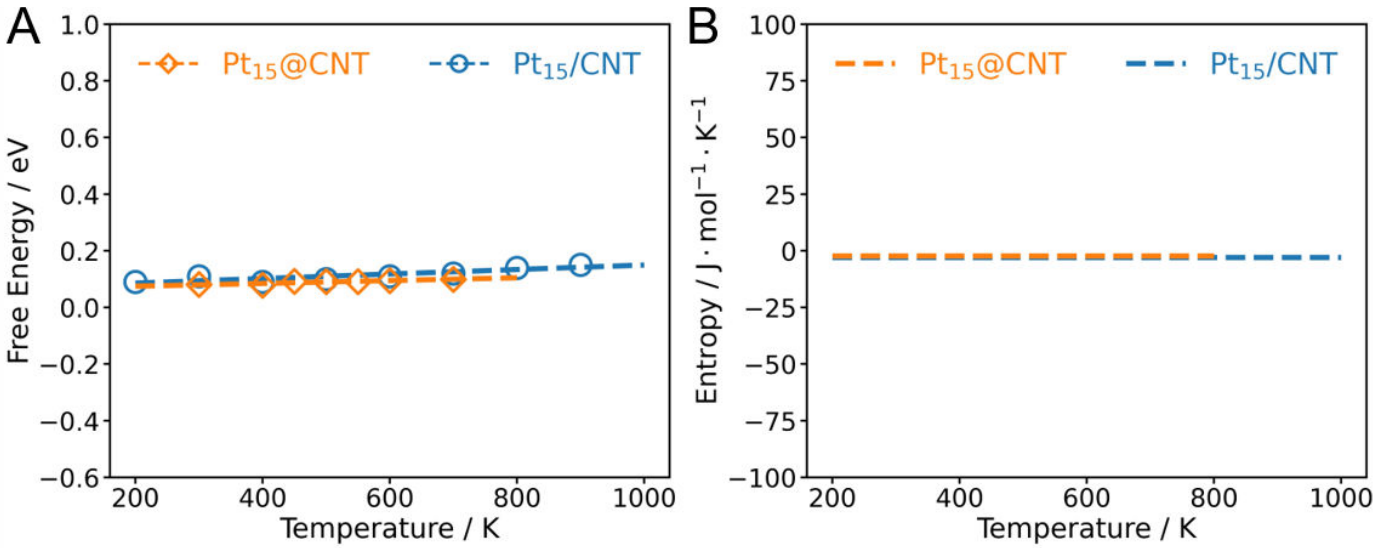

Fig. S 8 (A) The free energy barrier ($\Delta G^{\neq}$) of O_2 dissociation on Pt_{15}@CNT and Pt_{15}/CNT as a function of temperature. The points represent the calculated values, and the lines are corresponding fitted curves. (B) The activation entropy ($\Delta S^{\neq}$) of O_2 dissociation on Pt_{15}@CNT and Pt_{15}/CNT as a function of temperature.

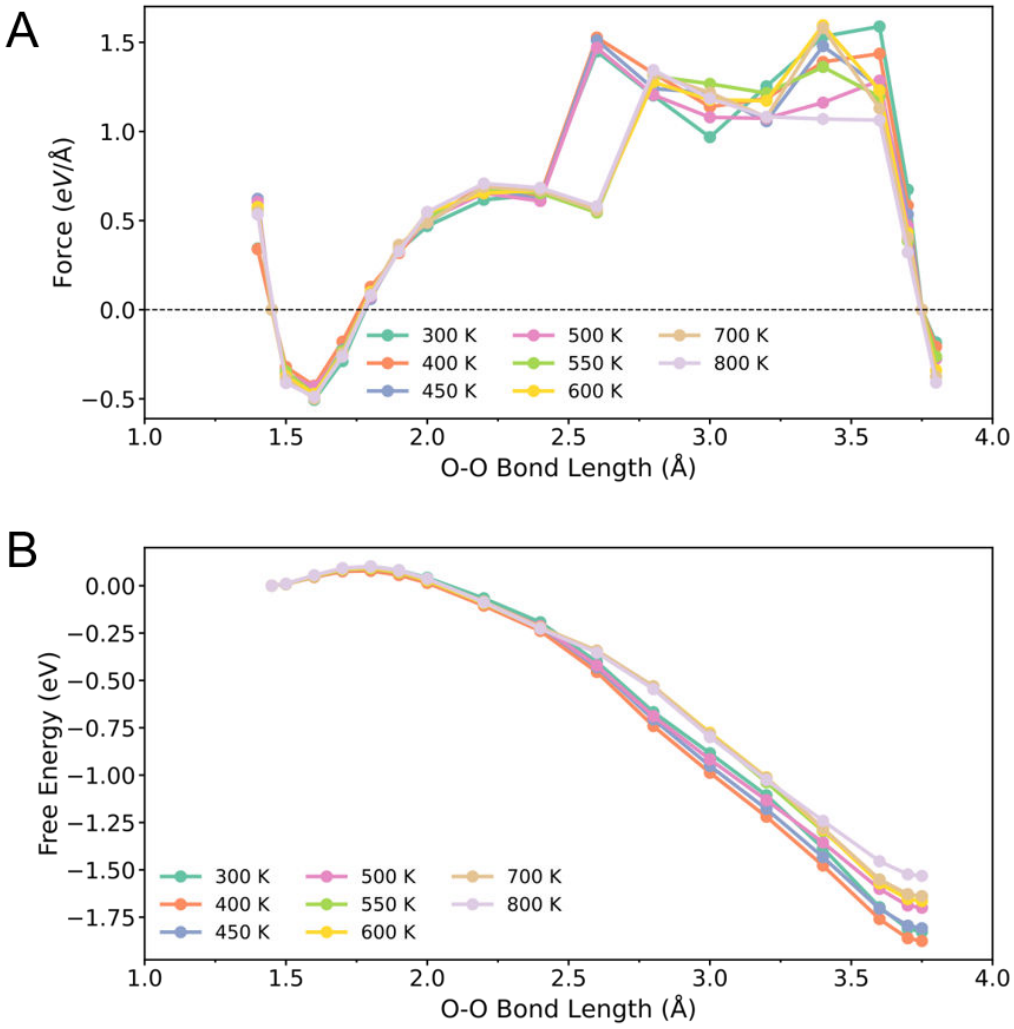

Fig. S 9 Calculated mean forces (A) and free energy profiles (B) of O_2 dissociation on Pt_{15}@CNT along the O-O bond length at different temperatures calculated using MLMD. The insets are the corresponding temperatures.

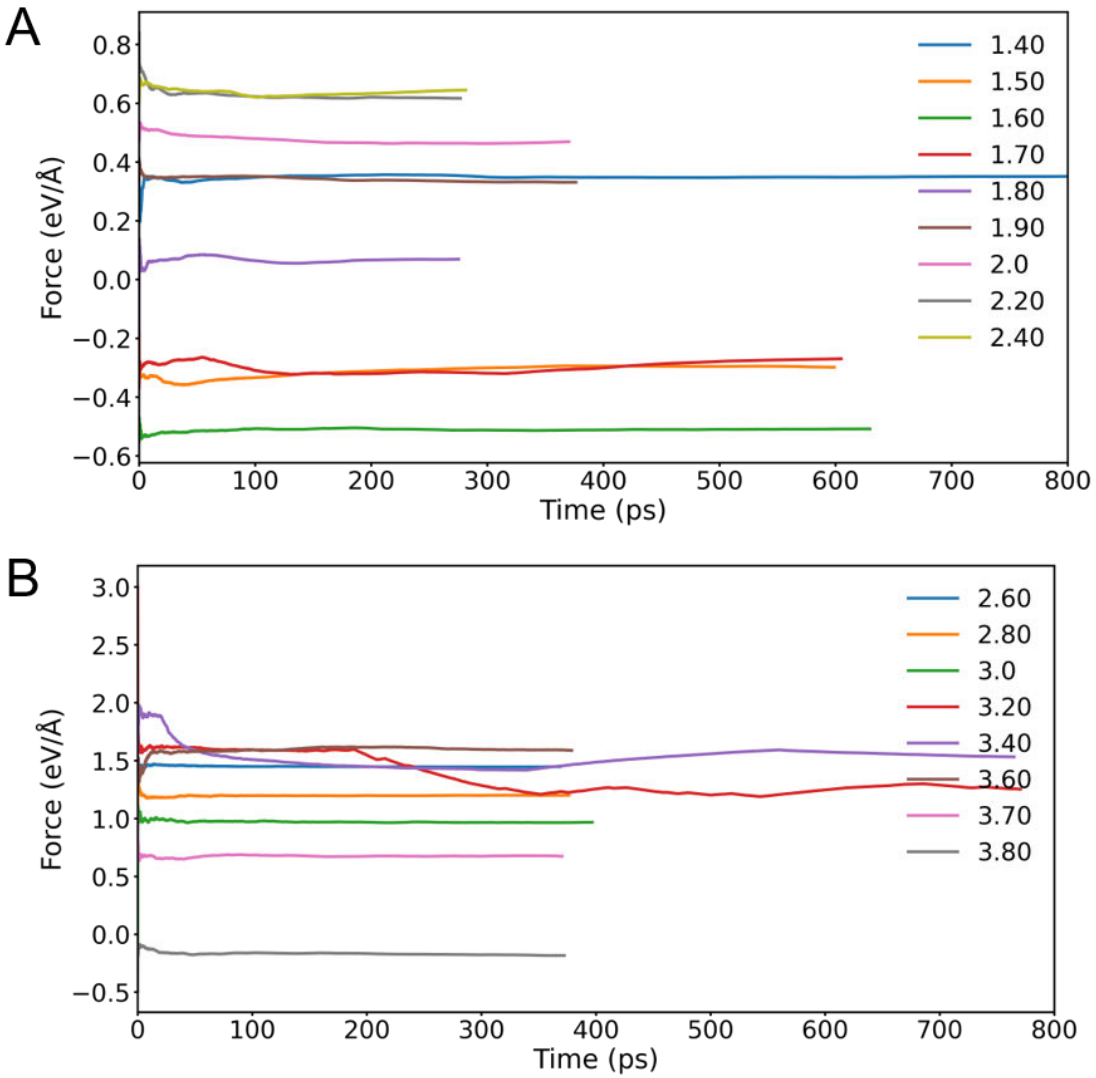

Fig. S 10 Time accumulative averages of the forces of O_2 dissociation on Pt_{15}@CNT at the O-O bond length varying from 1.40 to 2.40 Å (A) and 2.60 to 3.80 Å (B) at 300 K calculated by MLMD. The insets are O-O bond length given in Å.

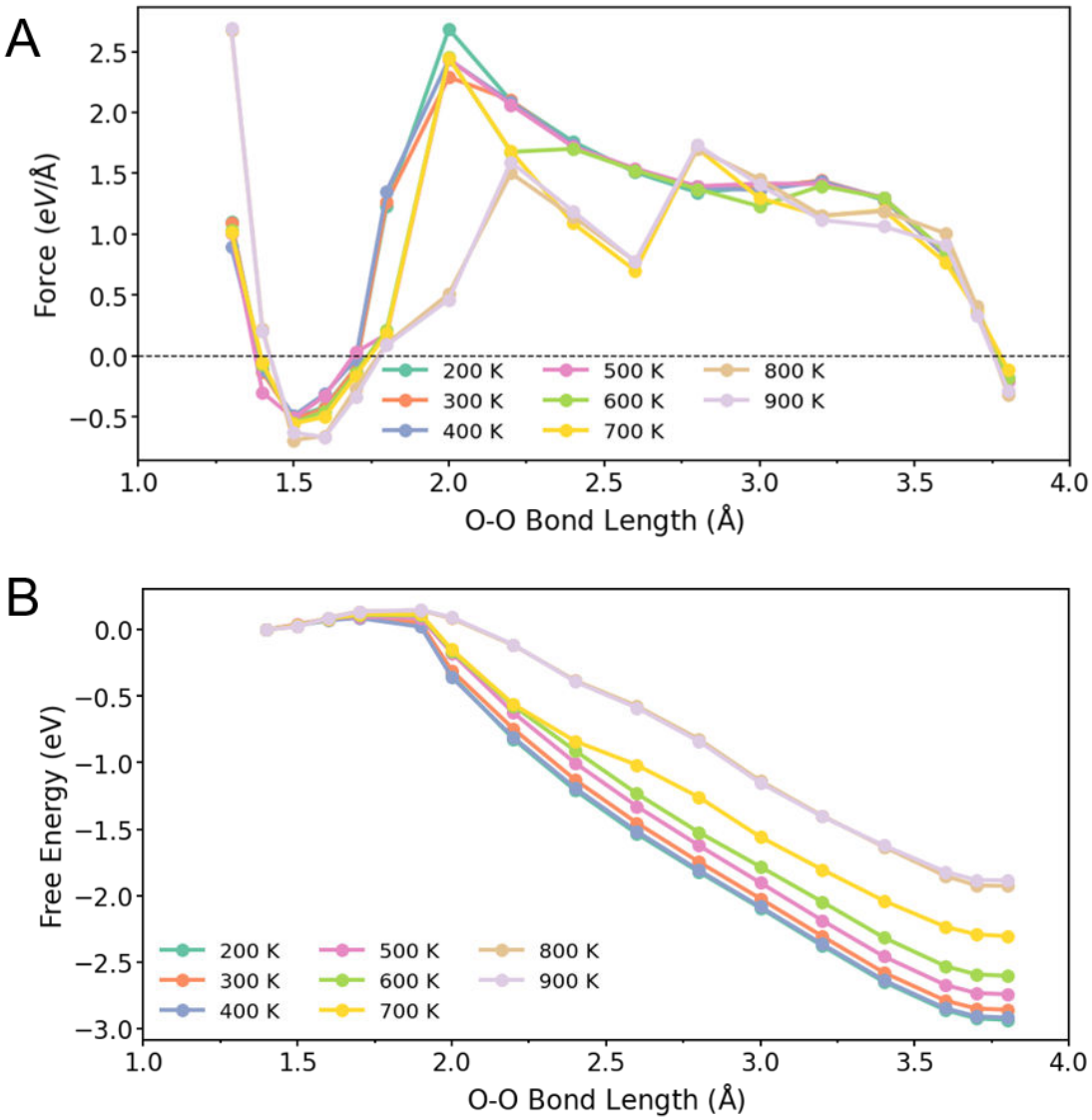

Fig. S 11 Calculated mean forces (A) and free energy profiles (B) of O_2 dissociation Pt_{15}/CNT along the O-O bond length at different temperatures calculated using MLMD. The insets are the corresponding temperatures.

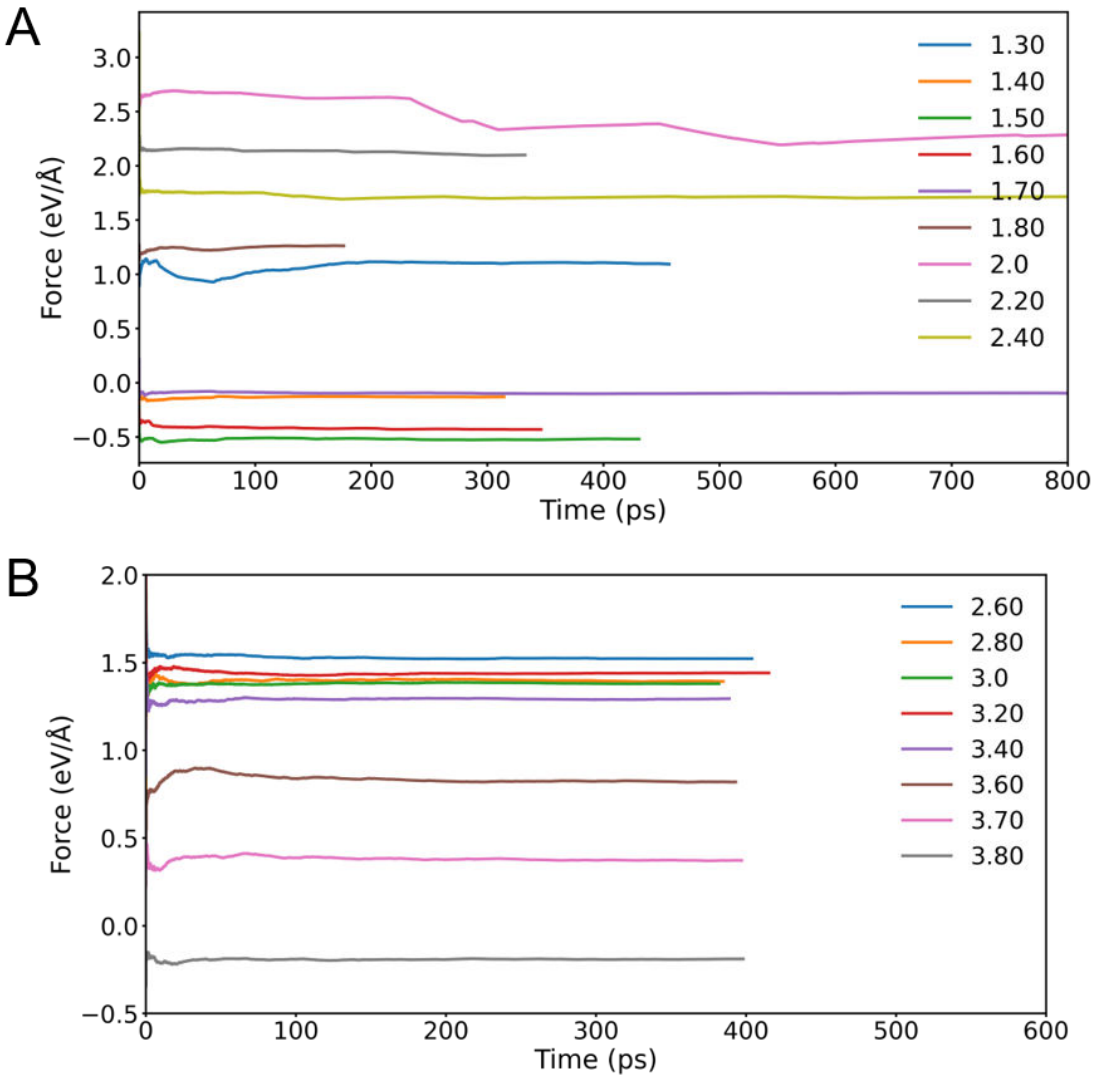

Fig. S 12 Time accumulative averages of the forces of O_2 dissociation Pt_{15}/CNT at the O-O bond length varying from 1.40 to 2.40 Å (A) and 2.60 to 3.80 Å (B) at 300 K calculated by MLMD. The insets are O-O bond length given in Å.

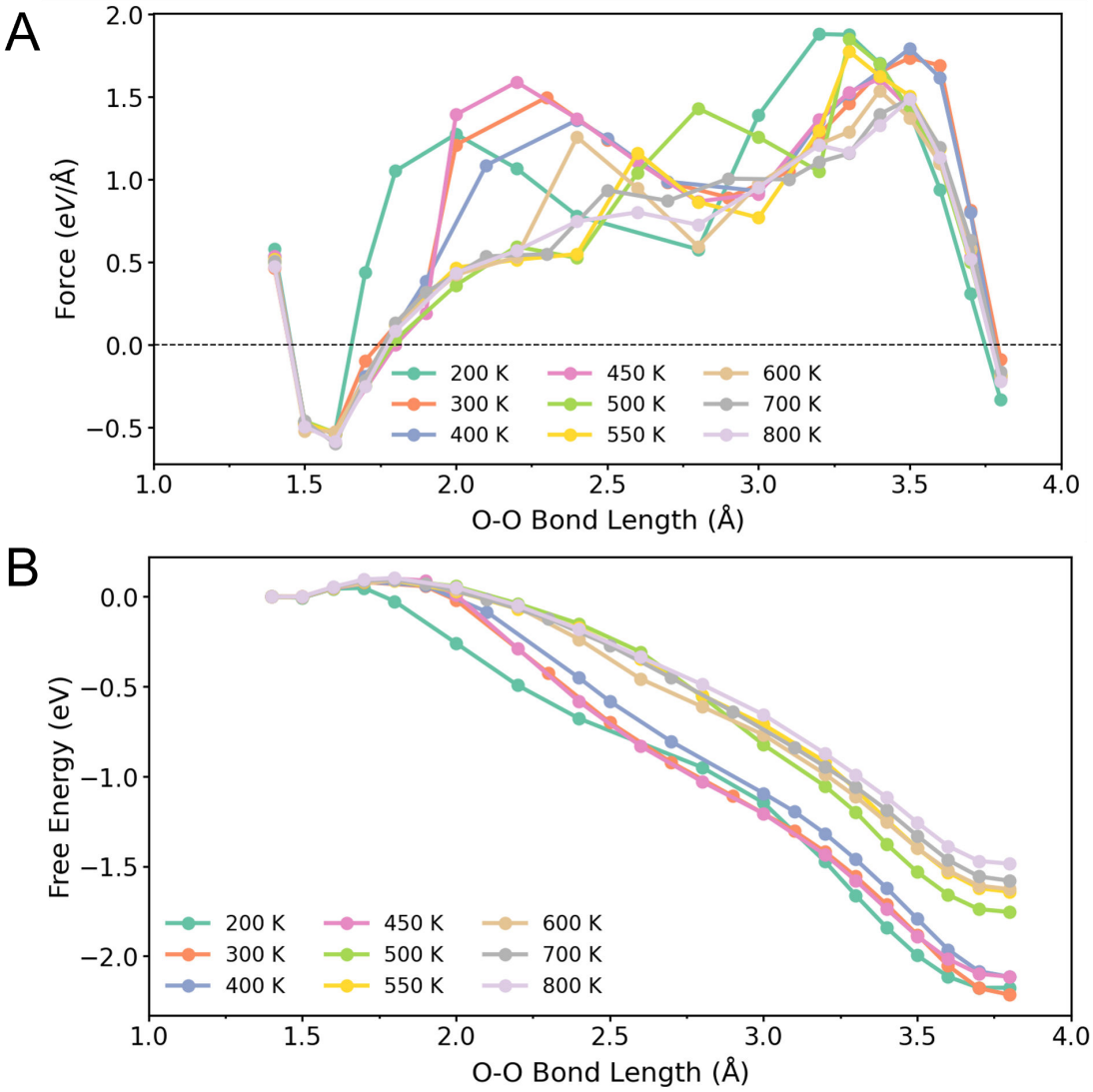

Fig. S 13 Calculated mean forces (A) and free energy profiles (B) of O_2 dissociation on Pt_{27}@CNT along the O-O bond length at different temperatures calculated using MLMD. The insets are corresponding temperatures.

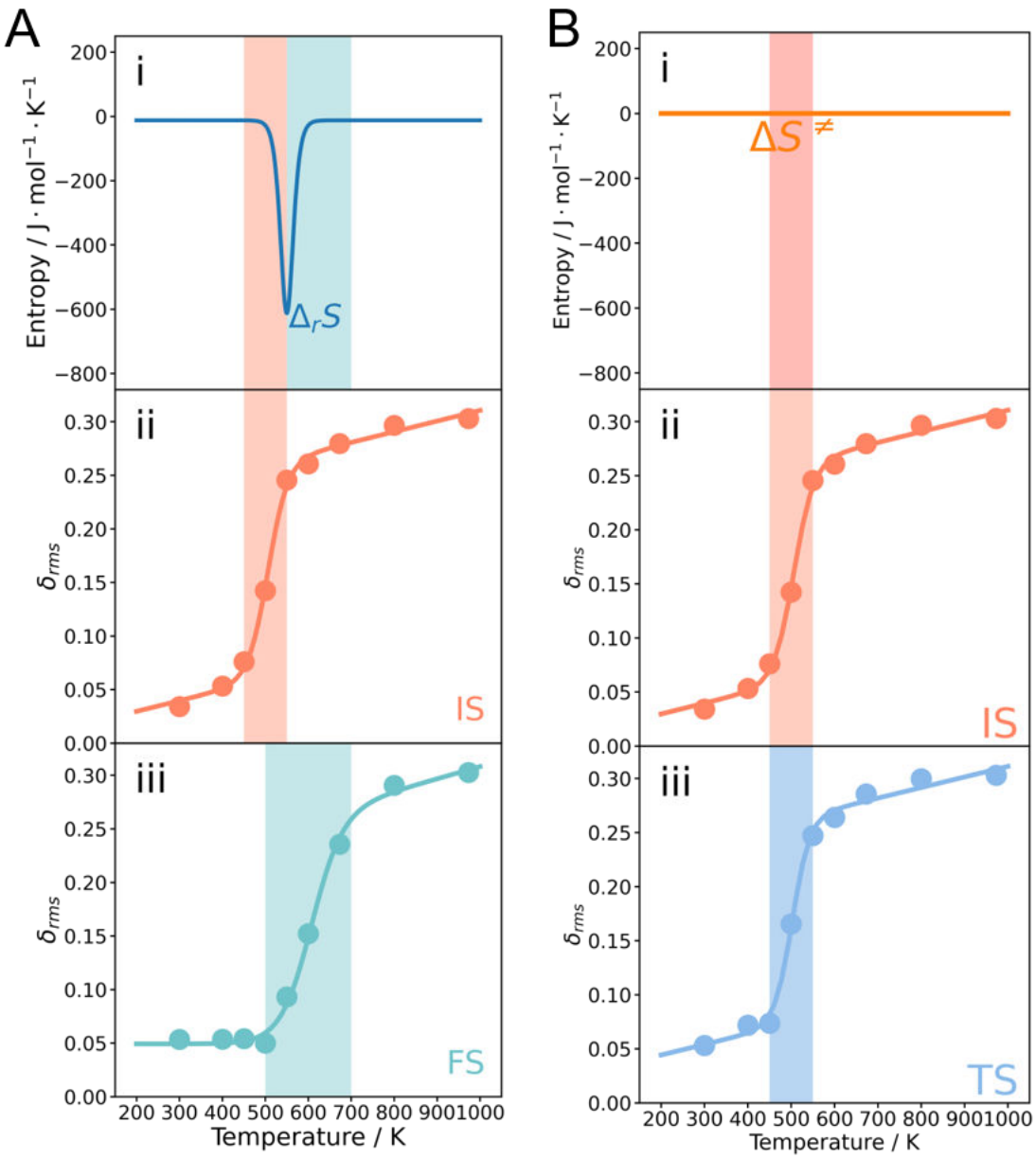

Fig. S 14 (A) Relation between the reaction entropy change ($\Delta_r S$) of O_2 dissociation on bare Pt_{15} and phase transitions of the IS and FS. (B) Relation between the activation entropy ($\Delta S^{\neq}$) of O_2 dissociation on bare Pt_{15} and phase transitions of the IS and TS. The colored regions indicate the solid and liquid coexistent state.

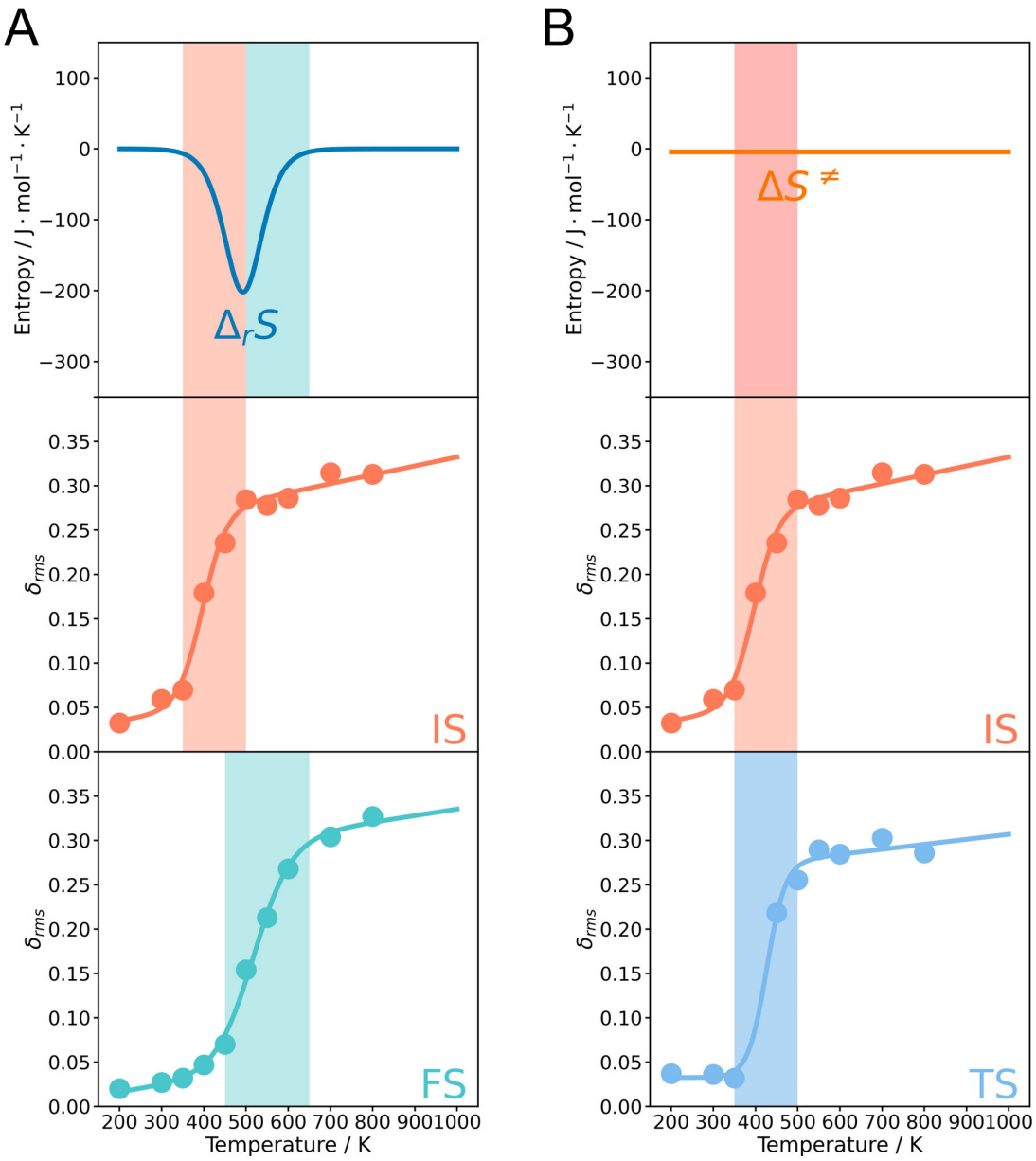

Fig. S 15 (A) Relation between the reaction entropy change ($\Delta_r S$) of O_2 dissociation on Pt_{15}@CNT and phase transitions of the IS and FS. (B) Relation between the activation entropy ($\Delta S^{\neq}$) of O_2 dissociation on Pt_{15}@CNT and phase transitions of the IS and TS. The colored regions indicate the solid and liquid coexistent state.

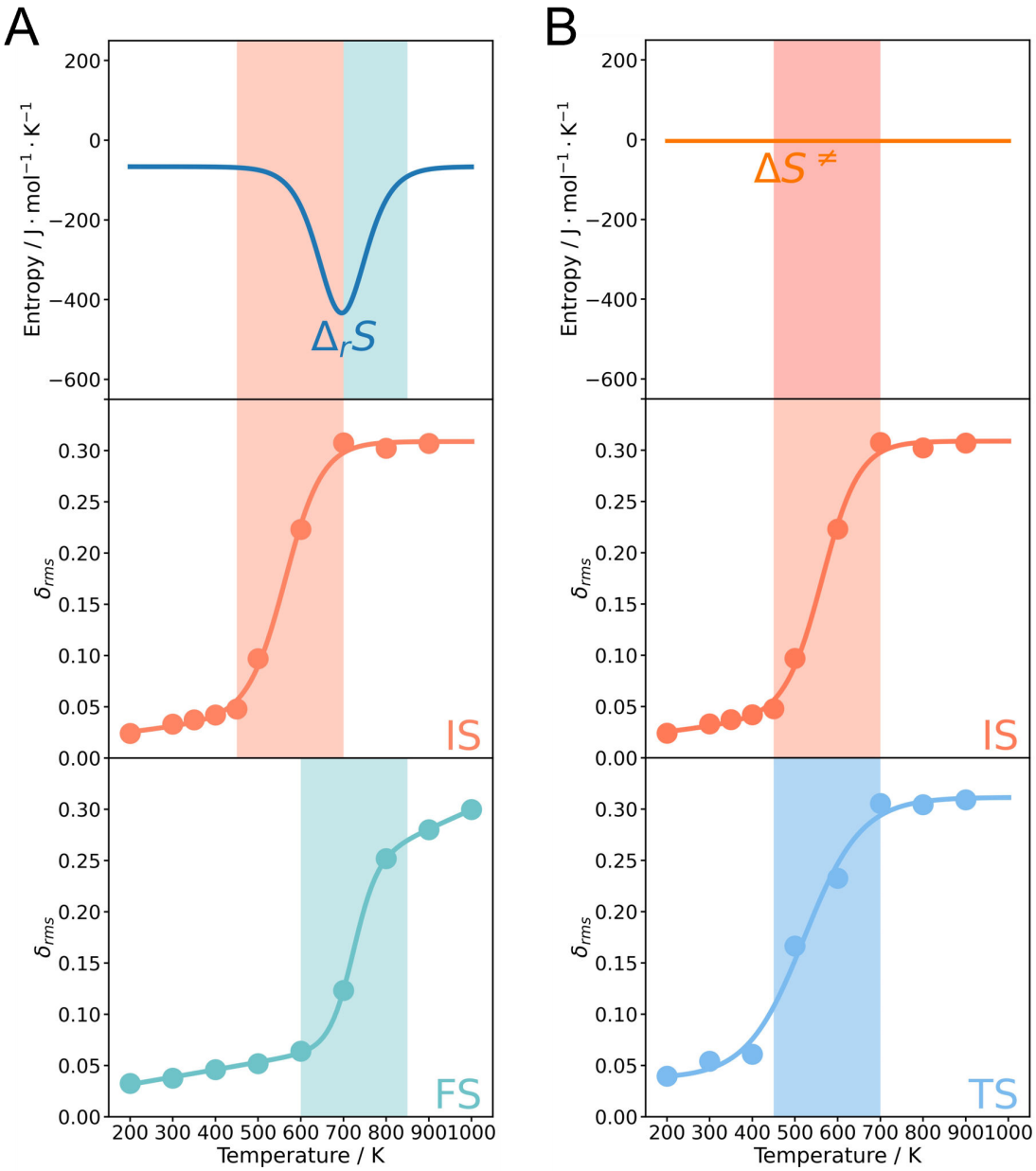

Fig. S 16 (A) Relation between the reaction entropy change (Δ_rS) of O_2 dissociation on the Pt_{15}/CNT and phase transitions of the IS and FS. (B) Relation between the activation entropy ($\Delta S^{\neq}$) of O_2 dissociation on the Pt_{15}/CNT and phase transitions of the IS and TS. The colored regions indicate the solid and liquid coexistent state.

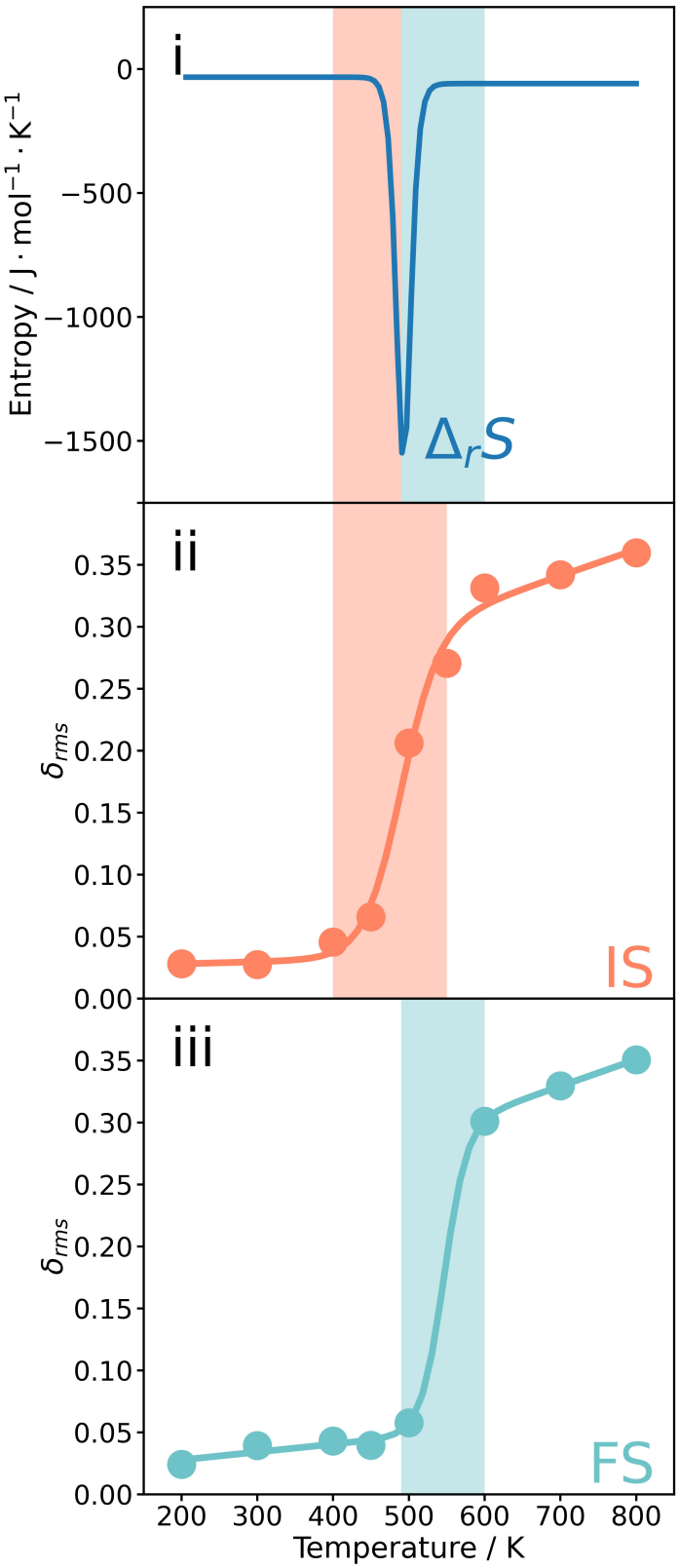

Fig. S 17 Relation between the reaction entropy change ($\Delta_r S$) of O_2 dissociation on the Pt_{27}@CNT and phase transitions of the IS and FS.

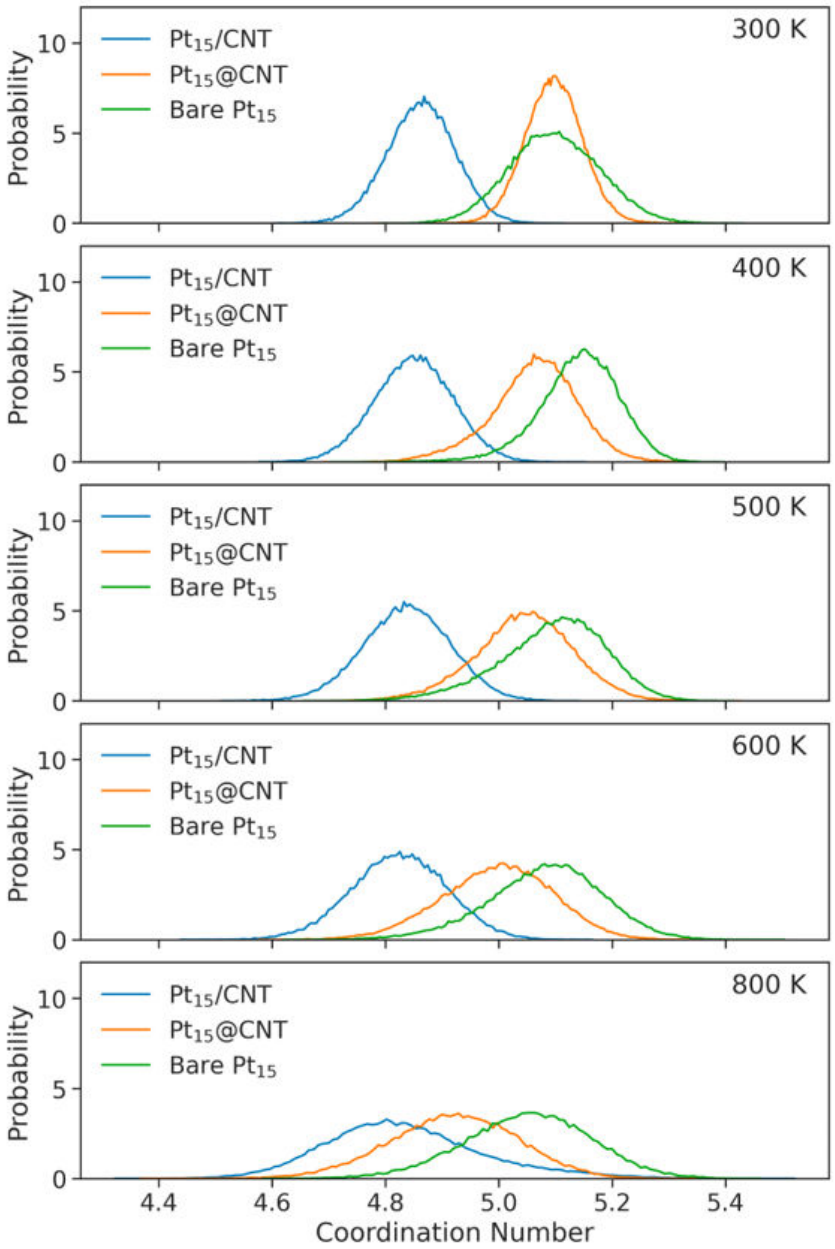

Fig. S 18 The probability distributions of average Pt-Pt coordination numbers of the bare Pt_{15}, Pt_{15}@CNT, and Pt_{15}/CNT at different temperatures. Note: For the supported clusters, they generally keep the solid-like structures when the temperature is less than 800 K. For these two-layer solid-like structures, there are four Pt atoms that have seven coordination numbers, and the other Pt atoms have quite low coordination. Especially for the Pt atoms at the terminal sites show the lowest coordination number. As a result, the average coordination number of the Pt cluster is relatively low.

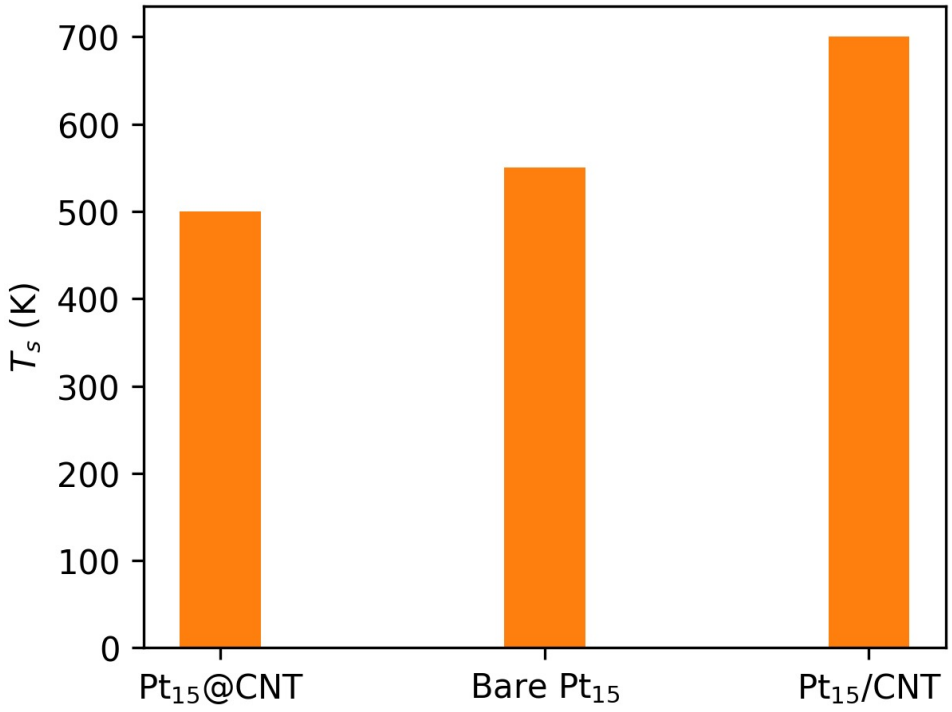

Fig. S 19 The temperature of peak position (T_s) in the $\Delta_r S$ curves for the Pt_{15}@CNT, bare Pt_{15}, and Pt_{15}/CNT.

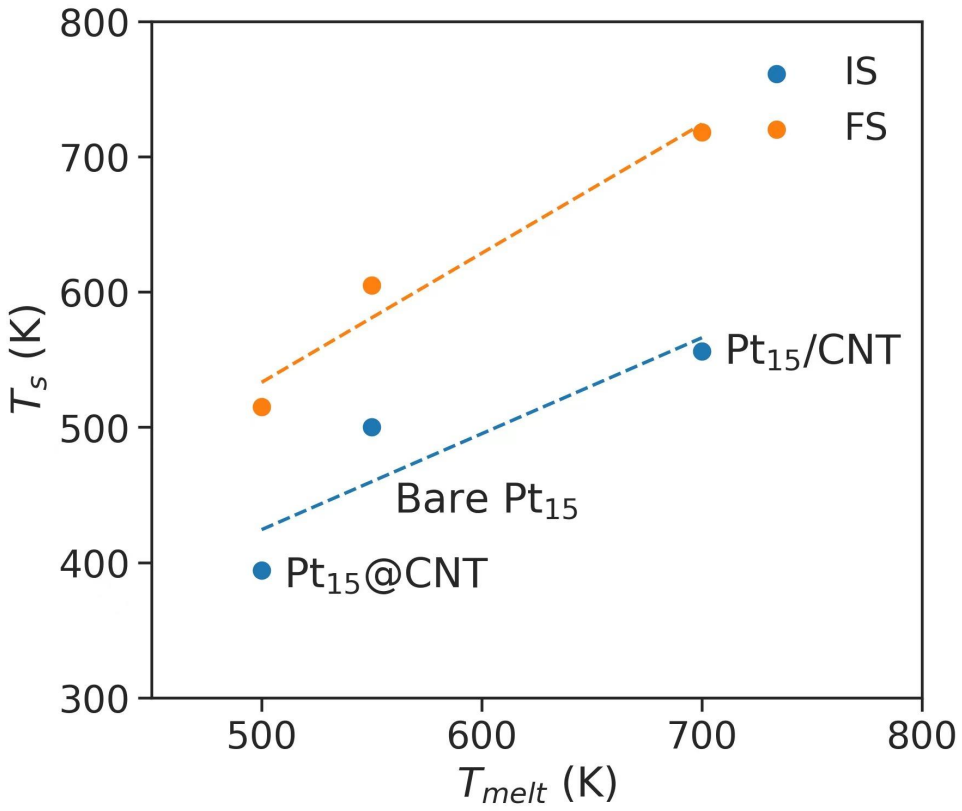

Fig. S 20 Correlation between the T_s and T_{melt} for the Pt_{15}@CNT, bare Pt_{15}, and Pt_{15}/CNT.

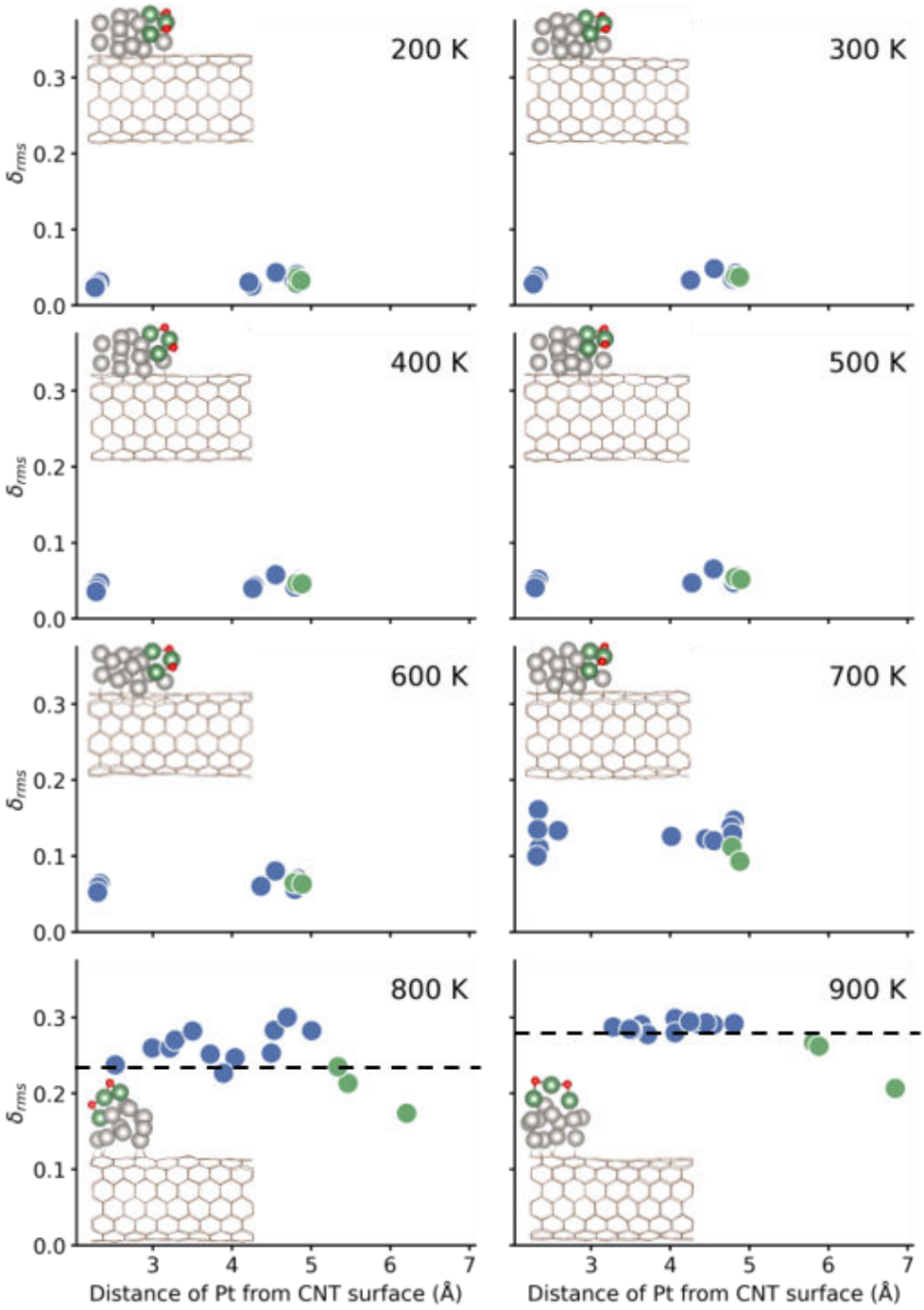

Fig. S 21 δ_{rms} of each Pt atom at the FS of the Pt_{15}/CNT as they vary with the distance of the Pt atoms from the CNT surface at different temperatures. The insets are the snapshots of structures from the MD trajectories. The silver and red balls are Pt and O atoms. The Pt atoms directly binding to the O atoms are highlighted in green.

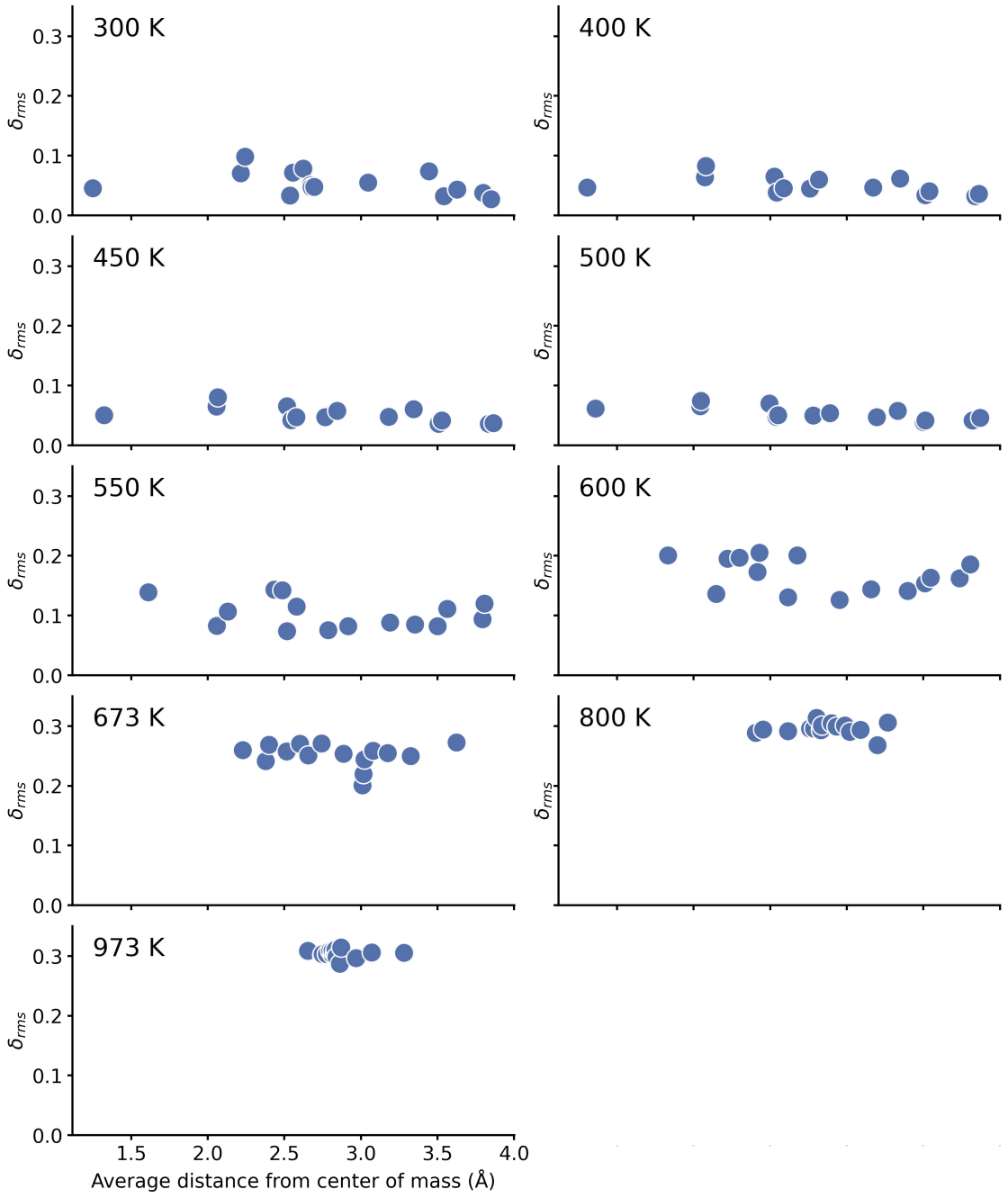

Fig. S 22 δ_{rms} of Pt atoms at the FS of the bare Pt_{15} as they vary with the distance of the atom from the center of mass of a cluster at different temperatures.

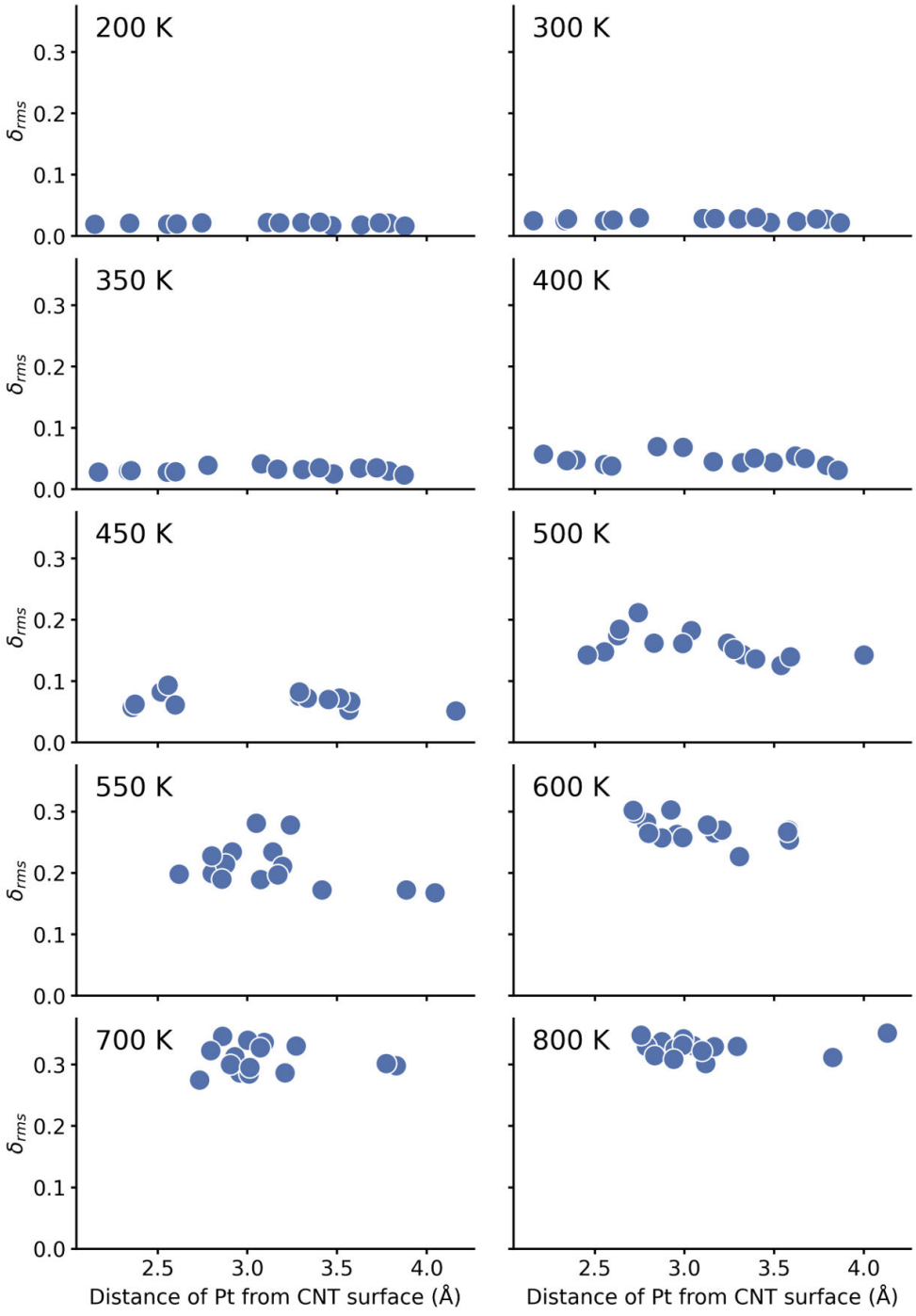

Fig. S 23 δ_{rms} of Pt atoms at the FS of the Pt_{15}@CNT as they vary with the distance of the Pt atoms from the CNT surface at different temperatures.

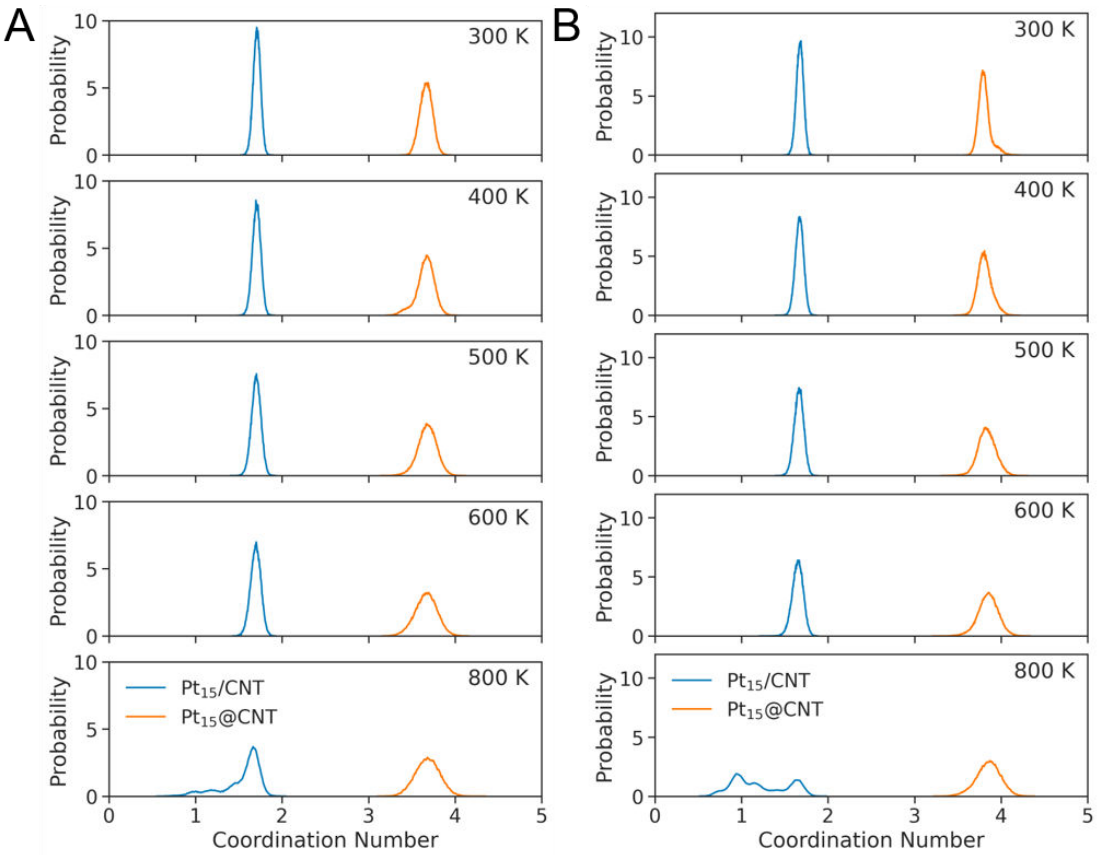

Fig. S 24 The probability distributions of average Pt-C coordination numbers of the FS (A) and IS (B) for the Pt_{15}@CNT and Pt_{15}/CNT at different temperatures.

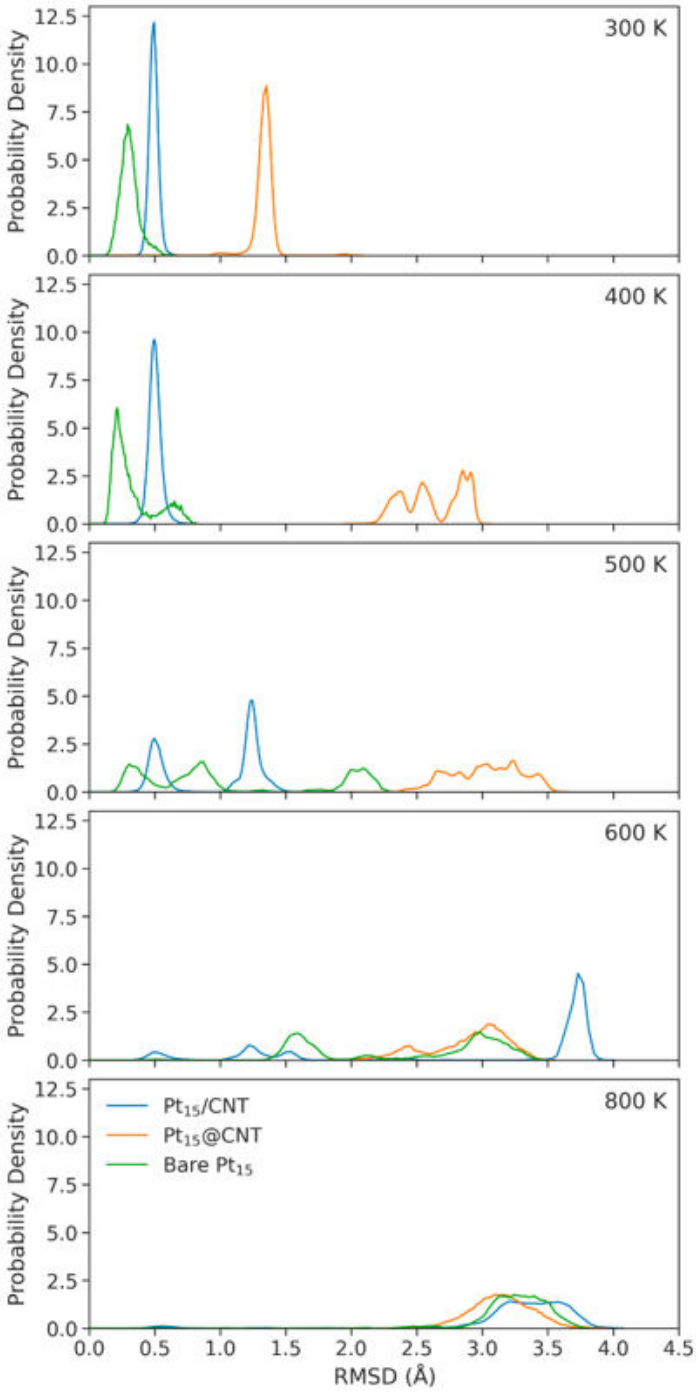

Fig. S 25 RMSD probability density of Pt atomic position at the IS for the Pt_{15}@CNT, Pt_{15}/CNT, and bare Pt_{15} at different temperatures. The RMSD of atomic positions is calculated along the MD trajectories with respect to the first frame.

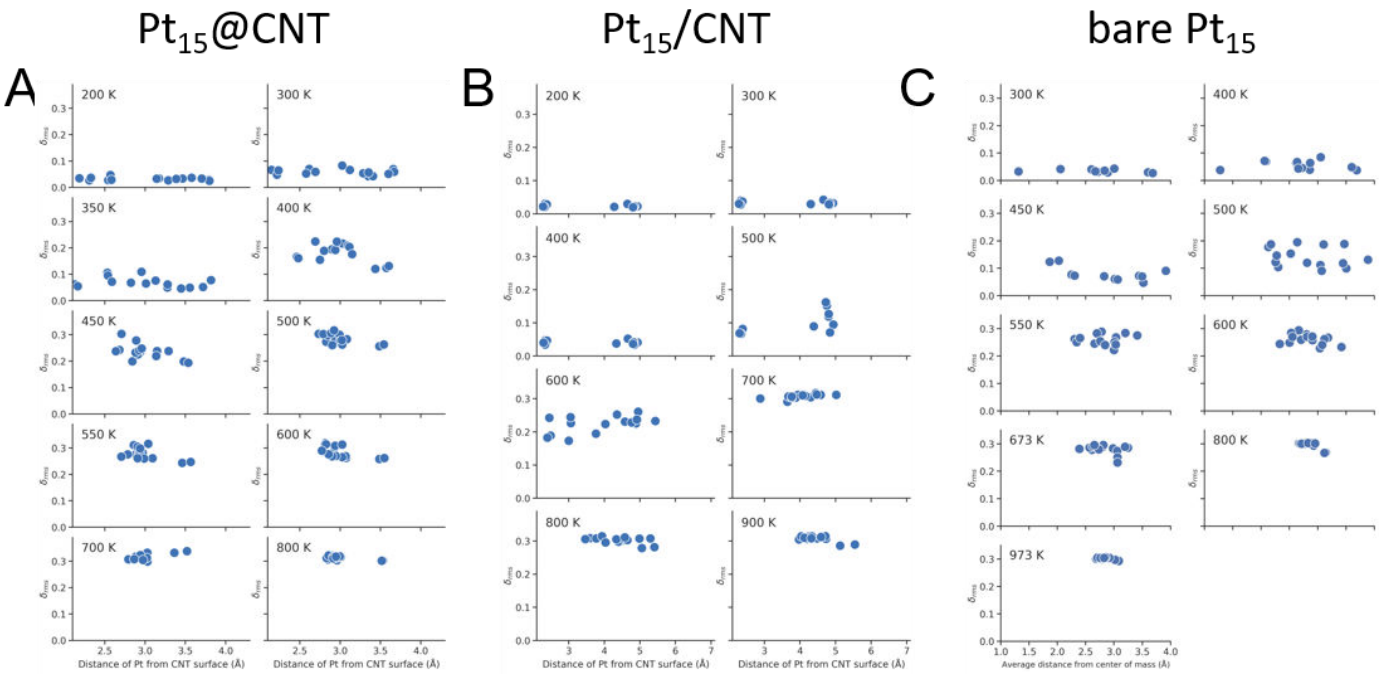

Fig. S 26 δ_{rms} of Pt atoms at the IS of the Pt_{15}@CNT (A), Pt_{15}/CNT (B), and bare Pt_{15} (C) at different temperatures.

Table S 1 The calculated O adsorption energies (E_O) of confined and supported Pt_{15} clusters using the traditional geometry optimization method.

	Pt_{15}@CNT	Pt_{15}/CNT
E_O (eV)	-4.6	-5.0

References

1 Y. Zhang, H. Wang, W. Chen, J. Zeng, L. Zhang, H. Wang and W. E, *Comput. Phys. Commun.*, 2020, **253**, 107206.
2 L. Zhang, J. Han, H. Wang, W. Saidi, R. Car and W. E, Advances in Neural Information Processing Systems, 2018.
3 L. Zhang, D.-Y. Lin, H. Wang, R. Car and W. E, *Phys. Rev. Mater.*, 2019, **3**, 023804.
4 G. Kresse and J. Furthmüller, *Comp. Mater. Sci.*, 1996, **6**, 15–50.
5 G. Kresse and J. Furthmüller, *Phys. Rev. B*, 1996, **54**, 11169–11186.
6 P. E. Blöchl, *Phys. Rev. B*, 1994, **50**, 17953–17979.
7 G. Kresse and D. Joubert, *Phys. Rev. B*, 1999, **59**, 1758–1775.
8 J. P. Perdew, K. Burke and M. Ernzerhof, *Phys. Rev. Lett.*, 1996, **77**, 3865–3868.
9 J. VandeVondele, M. Krack, F. Mohamed, M. Parrinello, T. Chassaing and J. Hutter, *Comput. Phys. Commun.*, 2005, **167**, 103–128.
10 E. A. Carter, G. Ciccotti, J. T. Hynes and R. Kapral, *Chem. Phys. Lett.*, 1989, **156**, 472–477.
11 G. Sun and H. Jiang, *J. Chem. Phys.*, 2015, **143**, 234706.
12 T. Cheng, H. Xiao and W. A. Goddard, *Proc. Natl. Acad. Sci. U.S.A.*, 2017, **114**, 1795–1800.
13 H. Li, C. Paolucci and W. F. Schneider, *J. Chem. Theory Comput.*, 2018, **14**, 929–938.
14 A. Barducci, M. Bonomi and M. Parrinello, *WIREs Comput. Mol. Sci.*, 2011, **1**, 826–843.
15 G. Bussi, D. Donadio and M. Parrinello, *J. Chem. Phys.*, 2007, **126**, 014101.
16 T. L. Beck, J. D. Doll and D. L. Freeman, *J. Chem. Phys.*, 1989, **90**, 5651–5656.
17 M. Iannuzzi, A. Laio and M. Parrinello, *Phys. Rev. Lett.*, 2003, **90**, 238302.
18 A. Vargas, G. Santarossa, M. Iannuzzi and A. Baiker, *Phys. Rev. B*, 2009, **80**, 195421.